

## Transport Mechanisms in the Outer Region of RFX-mod

E. Martines, A. Alfier, M. Agostini, A. Canton, R. Cavazzana, G. De Masi, A. Fassina, P. Innocente, R. Lorenzini, P. Scarin, G. Serianni, M. Spolaore, D. Terranova, N. Vianello, M. Zuin

Consorzio RFX, Associazione Euratom-ENEA sulla Fusione, Padova, Italy.

e-mail contact of main author: [emilio.martines@igi.cnr.it](mailto:emilio.martines@igi.cnr.it)

**Abstract.** The edge region of the RFX-mod reversed field pinch experiment is shown to possess good flux surfaces, thanks to the action of the feedback system for the control of MHD modes, although the presence of  $m = 0$  magnetic islands creates a complex magnetic structure. In Multiple Helicity conditions a localized plasma-wall interaction is still present, whereas when Quasi Single Helicity sets in a more widespread interaction takes place. Electron temperature profiles are determined by the  $m = 0$  islands, being flat inside them. The particle diffusion coefficient and the thermal conductivity are 10-20  $\text{m}^2/\text{s}$  and 100-200  $\text{m}^2/\text{s}$  respectively in low-current MH discharges. The edge temperature gradient is found to grow linearly with plasma current. The presence of a double velocity shear layer, already observed in the old RFX, is confirmed, and is shown to be determined by a nonlinear interplay with edge turbulence through the electrostatic Reynolds stress. A dependence of the flow velocity on the density normalized to the Greenwald density is also found. Edge turbulence features coherent structures, which have the form of a pressure peak associated to an eddy in the perpendicular plane and to a parallel current density filament. These structures have a prominent role in determining the cross-field particle transport.

### 1. Introduction

The Reversed Field Pinch (RFP) is a toroidal magnetic configuration which presents several attractive features. These include the fact that most of the magnetic field is created by currents flowing in the plasma itself, rather than in external coils, and the theoretical possibility of obtaining reactor-grade plasmas with ohmic heating only. Despite these advantages, the assertion of the RFP as a real alternative to the tokamak for building a simple low-cost reactor has been hindered in the past decades by the intrinsic high level of magnetic chaos, which limits the energy confinement capability. This is due to the dynamo effect, the MHD nonlinear process which transfers energy from the toroidal to the poloidal direction, sustaining the magnetic field reversal in the edge region against resistive diffusion. The dynamo process is achieved through the action of MHD  $m = 1$  tearing modes, which give rise to an effective electric field through the  $\mathbf{v} \times \mathbf{B}$  term in Ohm's law. However, the superposition of the magnetic islands of the dynamo modes destroys the magnetic surfaces, giving rise to a stochastic plasma core with poor confinement properties.

This picture, which is referred to as multiple helicity (MH) state, is now drastically changing. The RFP has been predicted since several years to be able to exist with only a single dynamo mode [1,2]. In this condition, dubbed single helicity (SH), the plasma would recover good magnetic surfaces, so that its confinement properties would be greatly improved. 3D MHD simulations have shown that a transition from MH to SH condition is indeed possible, when the dissipation properties of the plasma are changed [3]. From the experimental point of view, states with the dominance of the most internally resonant  $m = 1$  mode have been observed in the major RFP devices [4,5]. These conditions have been named quasi single helicity (QSH) states, due to the fact that the secondary modes still retain a finite amplitude. In particular, a special class of QSH states, called single helical axis (SHAx) states, has been recently characterized in the RFX-mod device [6]. In these states the O-point corresponding to the main magnetic axis and the island X-point collapse one onto the other, the island separatrix is expelled from the plasma and the island O-point survives as the main

magnetic axis of a spontaneously occurring helical plasma. The new state is more resilient to magnetic chaos, due to the disappearance of the X-point [7].

In this paper we present an overview of experimental results regarding the transport processes in the outer region of the RFX-mod experiment ( $R = 2$  m,  $a = 0.459$  m) operating in Padova (Italy) [8]. The understanding of edge transport is crucial in MH plasmas, where the edge is the only region where conserved magnetic surfaces exist, and gradients of density and temperature can develop. Also in QSH states, however, where the core plasma improves its confinement properties, strong gradients exist at the edge, so that this region is important for the overall discharge performance. Furthermore, the edge region determines the plasma-wall interaction, which has been for a long time a major problem in the route towards high current operation in RFX-mod, and will be a crucial issue for next generation RFPs.

The RFX-mod device is an improved version of the old RFX machine. The most innovative feature is the presence of a system of 192 saddle coils located outside of the vacuum vessel and covering the whole plasma surface. The coils are feedback controlled using 192 sensors measuring the radial component of the magnetic field, and can act so as to minimize this field, thus mimicking the effect of a perfectly conducting shell (the machine is also equipped with a copper shell with a time constant for vertical field penetration of 50 ms). This system has drastically changed the performance of the device, reducing the amplitude of the dynamo modes at the plasma boundary and consequently alleviating their phase-locking and wall-locking. This has improved the plasma-wall interaction. It is worth mentioning that in RFX-mod there are no limiters or divertors, and the plasma interacts directly with the first wall, which is covered by graphite tiles in order to bear the heat load.

## 2. Magnetic topology of the outer region

The outer region of RFP plasmas is dominated by the presence of magnetic islands due to the  $m = 0$  modes which are resonant on the reversal surface. Depending on the value of the reversal parameter, the islands can intercept the first wall (for shallow reversal, around  $F = -0.05$ ) or not (deep reversal, around  $F = -0.2$ ). Furthermore, the  $m = 0$  tend to phase lock to each other [9]. The typical phase relationship is  $\alpha_{0,k} = k\phi_L - \phi^*$ , where  $\phi_L$  is the toroidal angle where the  $m = 1$  modes lock to the wall, and  $\phi^* \approx \pi/2$ . This phase relationship leads to a funnel-like shape of the plasma column.

In order to accurately assess the plasma edge structure the magnetic field line path can be reconstructed using the FLiT code [10]. FLiT integrates the magnetic field line equation using the magnetic field values given by a reconstruction of the eigenmodes into the plasma based on Newcomb's equation in toroidal geometry, supplemented with magnetic field measurements at the plasma edge [11].

A typical Poincaré plot of the magnetic field on the outer horizontal plane ( $\theta = 0$ ) in MH condition is shown in the left panel of Fig. 1, for  $r > 0.3$  m. It is possible to observe the inner stochastic region, due to the superposition of  $m = 1$  mode islands, which extends up to  $r/a = 0.38$  m approximately. Beyond this region lies the chain of the  $m = 0$  magnetic islands. Here a higher degree of order, with good magnetic surfaces, is recovered. However, the island structure short-circuits the two boundaries of this region, similar to what happens in tokamaks when NTM-induced islands develop. The consequence of this on the plasma profiles will be discussed in the next section. Before and after the  $m = 0$  islands, two regions of conserved magnetic surfaces exist, extending a few cm radially. These surfaces are distorted by the effect of the  $m = 1$  mode locking and by the funnel-like shape induced by the  $m = 0$  phase locking. It is worth noting that it may be that the surfaces located more internally than the  $m = 0$  islands are not as good as they appear from the figure, since the mode reconstruction works only for  $n < 24$ , due to the limited number of magnetic measurements at the edge:

therefore, the influence of  $m = 1$  modes resonant near the reversal surface may have been underestimated. Depending on the degree of phase locking, on the mode amplitude, and on the value of the reversal parameter  $F$  (which determines the location where the  $m = 0$  modes resonate), the interaction of the plasma with the first wall can take different forms. In particular, the  $m = 0$  islands heavily intercept the first wall at shallow reversal, ruling out any effect of the outermost magnetic surfaces, while such surfaces may play a role in confining the outer plasma region at deeper  $F$  (as in the case of Fig. 1). In any case, the high degree of phase locking gives rise to a toroidally localized plasma-wall interaction, as seen in the figure, only partially alleviated by the mode amplitude reduction produced by the feedback system.

The situation outlined above changes when a QSH state develops. An example of Poincaré plot in this condition is shown in the right panel of Fig. 1. It can be seen that, apart from the

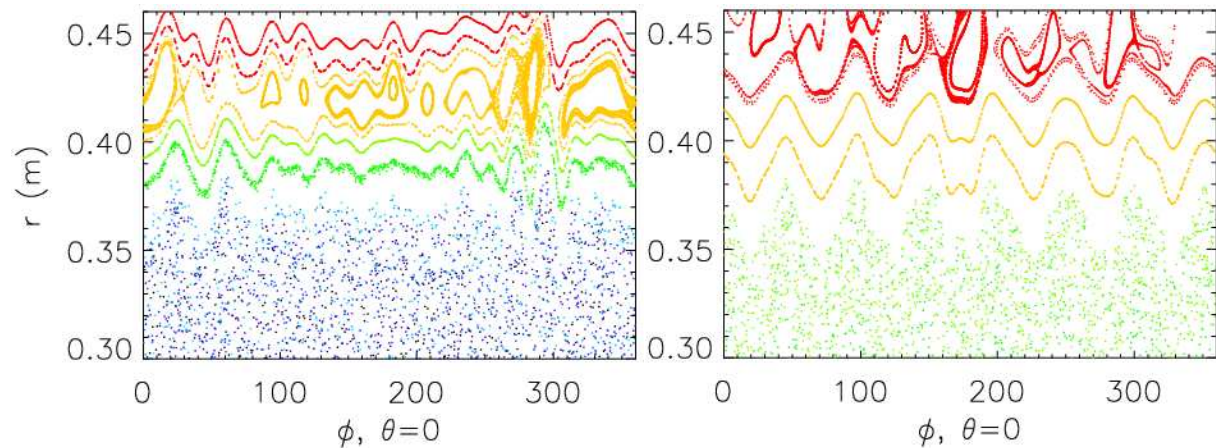


**Fig. 1: Poincaré plots on the  $r$ - $\phi$  plane of the magnetic field lines for a MH helicity condition (left) and for a SHAx state (right). The region  $r > 0.3$  m is displayed, so as to better show the edge region.**

appearance of the  $n = 7$  helical structure in the plasma core, which is outside of the graph boundaries, the reduction of the secondary mode amplitude makes the region of conserved flux surfaces before to the  $m = 0$  island chain more regular, with a clear  $n = 7$  modulation. Another important feature is the regularization of the plasma-wall interaction, which is now regulated by the  $m = 0$  islands intercepting the wall in several toroidal positions. This role of the  $m = 0$  islands is also due to the fact that high current operation, where SHAx states appear, has been carried out preferentially at shallow values of the reversal parameter  $F$ .

It is interesting to compare these results with those published in ref. 12, which refer to the old RFX, without the feedback system for the control of MHD modes and with a thicker shell. In that case the outer region flux surfaces were found to be partially destroyed, so that a direct connection of the edge plasma to the first wall was present. With the feedback system the situation is now very different: good magnetic surfaces are present beyond the  $m = 0$  island chain, so that no stochastically wandering field lines intercept the first wall. Furthermore, good surfaces are found also on the other side of the island chain in high current SHAx states. The old situation is partially recovered during discrete reconnection events, when a temporary stochastization of the outer region takes place [13].

### 3. Particle and energy transport in the low-current MH regime

Low current (300-400 kA) discharges are particularly suited to study the edge features in RFX-mod, thanks to the possibility of inserting electric probes, which are a simple yet effective method for measuring density and temperature profiles. Fig. 2 shows electron temperature data obtained using a balanced five-pin triple probe, which has been inserted into the edge plasma (up to  $x = +50$  mm from the first wall convolution) on a shot-by-shot basis.

They are combined with Thomson scattering measurements, showing the good agreement of the two diagnostics. The Thomson scattering data are actually measured on the inboard side, and then traced to the probe location using the FLiT code and assuming constant temperature along field lines. The resulting temperature profile displays a double gradient with a plateau located in the region  $360 < r < 410$  mm. The origin of this plateau can be understood by looking at the Poincaré plot computed by the FLiT code on the radial-toroidal outboard plane, also shown in Fig. 2, where a blue line marks the position at which the profile is measured. It can be seen that the temperature plateau is due to the presence of an  $m = 0$  island, which short-circuits different radial positions, equalizing the temperature (no energy sources are present in this region). This is a behavior similar to that induced in tokamaks by NTM islands.

The measured density and temperature profiles have been used to compute the particle diffusion coefficient and the electron thermal conductivity in the outer region, as shown in Fig. 3. The diffusion coefficient, computed using the particle flux driven by the

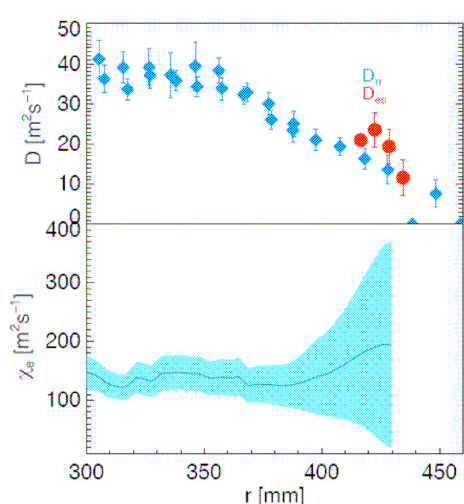


**Fig. 3:** Top: diffusion coefficient measured by probes (red) and estimated according to theory of transport in a stochastic magnetic field (blue); Bottom: Computed thermal diffusivity, with a shaded region marking the uncertainty.

electrostatic turbulence (red points), is found to be in the range  $10\text{-}20$   $\text{m}^2/\text{s}$  in the last few cm. On the same graph is plotted the value expected according to the Harvey formula for transport in a stochastic magnetic field [14], computed using the reconstructed radial field amplitude for large scale tearing modes (blue). The experimental points due to the electrostatic turbulence, which is indeed known to be responsible for particle transport in the RFP edge, are found to be consistent with the stochastic transport which could take place deeper into the plasma.

The thermal conductivity, computed using the average energy flux, is of the order of  $100$   $\text{m}^2/\text{s}$ , with a relatively flat profile over the whole edge region. This is substantially lower than what would be expected from magnetic field stochasticity, confirming the idea that good magnetic surfaces exist in the outer region of the RFP configuration.

#### 4. Energy transport in high-current SHAx states

As shown by the Poincaré plots displayed in section 2, QSH states, and in particular the newly found SHAx states, display a higher degree of magnetic order. This results also in a more ordered plasma-wall interaction. This is confirmed by measurements of floating potential performed with a toroidal array of 72 Langmuir probes embedded in the graphite tiles, which are part of the Integrated System of Internal Sensors (ISIS) [15]. The probes are located at the poloidal angle  $\theta = 341^\circ$ , i.e. slightly below the outer equator. An example of the

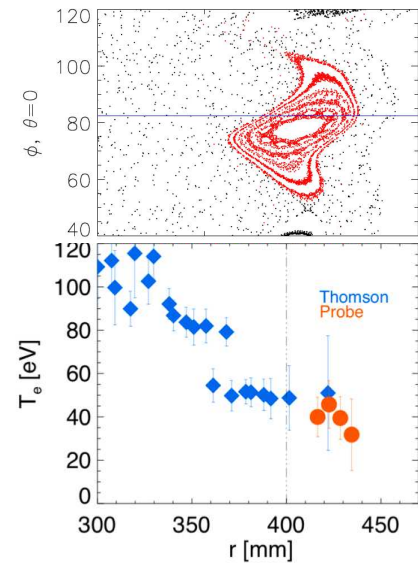


**Fig. 2:** Poincaré plot in the  $r$ - $\phi$  plane, with a blue line marking the line of sight of the Thomson scattering (top), and temperature profile given by Thomson scattering (blue) and probe (orange) data.

floating potential toroidal pattern detected by these probes during the SHAx states is shown in Fig. 4. It is clearly seen an  $n=7$  modulation, having an amplitude of the order of 10 V. The origin of this modulation could be attributed either to the plasma potential pattern associated to the mode, or to the  $n=7$  modulation of the plasma-wall interaction.

By using Thomson scattering data, the near edge (34-40 cm) temperature gradient has been evaluated as a function of plasma current. The result is shown in the left panel of Fig. 5, which shows a linear trend in the whole range 0.3-1.5 MA of currents explored by RFX-mod up to now. In the same panel is also shown the gradient for the far edge (42-45 cm) obtained with a Thermal Helium Beam (THB) diagnostic, which uses the He line intensity technique [16] to measure the local electron temperature and density radial profiles. The data pertaining to MH and SHAx conditions are mixed in the graph, as no clear difference could be found between the two sets. This is in agreement with the fact that the transition to the SHAx state has a strong effect on the core confinement, favoring the development of a steep temperature gradient in that region, while the edge profiles are almost unaffected.

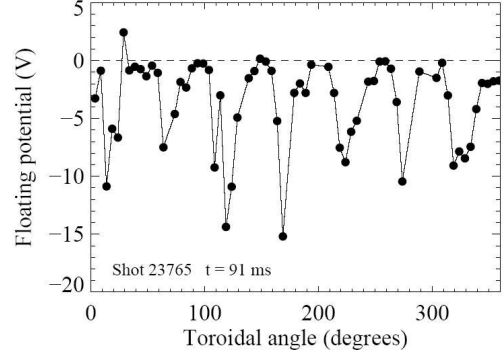


**Fig. 4: Floating potential as a function of  $\phi$  measured by probes embedded in the first wall in a SHAx state.**

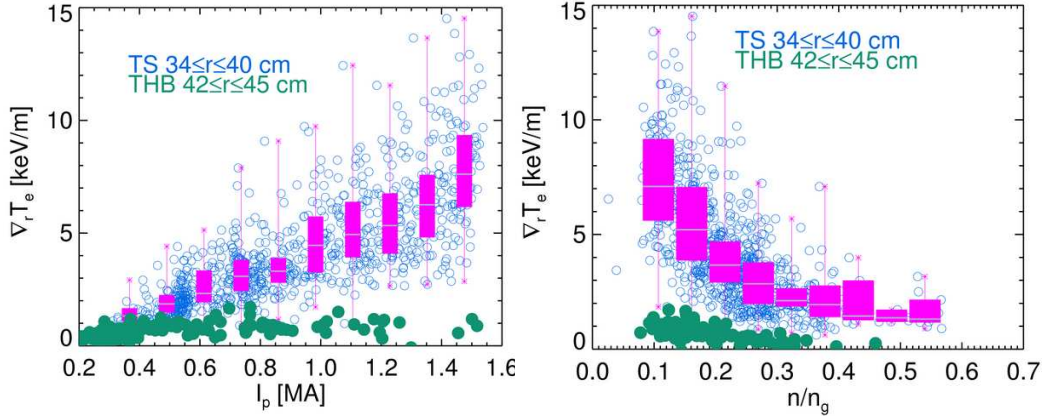


**Fig. 5: Edge electron temperature gradient plotted as a function of plasma current (left) and of normalized density (right), for the near edge (open circles) and for the far edge (full circles). The purple bars represent averages and standard deviations of the near edge data.**

The dependence of the edge temperature profile on the ratio between density  $n$  and Greenwald density  $n_G$  is shown in the right panel of Fig. 5, both for the near and far edge. A strong dependence can be observed, with steeper gradients found at low density, and a tendency to saturate for  $n/n_G > 0.4$ .

## 5. Flow profiles and momentum transport

The plasma flow profiles have been investigated in RFX-mod low-current discharges using two different types of insertable probes. One of them, a Gundestrup probe [17], measures the plasma flow velocity components in directions parallel and perpendicular to the magnetic field (poloidal and toroidal in the RFP edge). The probe has been used with all the pins collecting floating potential signals, and the flow has been reconstructed according to a suitable model [18]. The other, dubbed U-probe, allows to evaluate the toroidal  $\mathbf{E} \times \mathbf{B}$  flow profile and to estimate the Reynolds and Maxwell stresses and their radial profiles. The typical perpendicular (toroidal) plasma flow profiles measured by the Gundestrup probe are

shown in the top panel of Fig. 6. The graph displays the Mach number, that is the plasma velocity normalized to the ion sound speed. As in the old RFX [19], the perpendicular velocity displays a double shear: a first shear region is located more or less across the  $r = a$  surface, whereas a second shear is found deeper into the plasma. For comparison, in the same figure the radial  $\mathbf{E} \times \mathbf{B}$  velocity profile obtained in another set of discharges is shown. The two profiles display a quite good agreement, taking into account possible toroidal asymmetries and slightly different discharge conditions.

The generation of a sheared perpendicular flow profile has been explained in RFPs through the turbulent Reynolds stress [20]. Despite the high level of magnetic turbulence, electrostatic fluctuations seem to play a fundamental role in driving the flow at the edge, being the Reynolds stress gradient larger than the Maxwell stress one. As a further confirmation the contribution  $\langle v_r M_\perp \rangle$ , reconstructed using the Gundestrup probe, is shown in the bottom panel of Fig. 6. As a comparison, the radial profile of  $\langle v_r v_\phi \rangle$  calculated from the U-Probe in a different set of discharges is also shown. The strong gradient in the innermost shear region is confirmed in both case, thus confirming the role of Reynolds stress in driving the plasma flow at the edge.

Another measurement of the edge toroidal turbulence propagation velocity  $v_\phi$  is given by the GPI diagnostic [21], which looks at the HeI emission along 16 lines of sight covering a limited region of the outer plasma. The velocity is evaluated through a cross-correlation of the signals. A toroidal propagation of emission bursts in the direction opposite to plasma current, the same as  $\mathbf{E} \times \mathbf{B}$  drift flow [22] is found. In Fig. 7 the scaling of  $v_\phi$  measured by the GPI with the normalized density  $n/n_G$  is shown for MH discharges; each black point is an average over 10 ms during the current flat-top. It can be seen that the velocity is higher at lower density, and then decreases, reaching a saturation level of 15 km/s at  $n/n_G \approx 0.35$ . The fluctuation velocity has been found in the past to be experimentally consistent, both in direction and absolute value, with the  $\mathbf{E} \times \mathbf{B}$  drift obtained from the radial gradient of plasma potential [23] and so it is often used as a proxy for the fluid velocity. The trend of  $v_\phi$  vs  $n/n_G$  is not an effect of the electron density only, but also of the plasma current. A possible explanation of this behavior could come from the balance between ion collisions and finite Larmor radius losses.

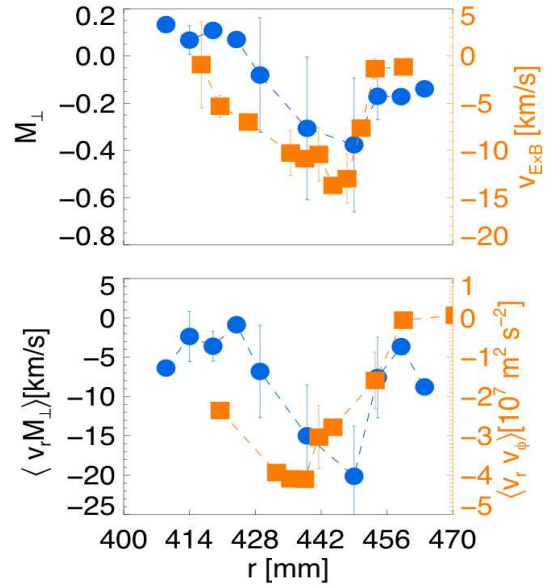


**Fig. 6: Top: Profiles of the perpendicular Mach number measured by the Gundestrup (blue) and of the EB velocity measured by the U-probe (orange); Bottom: Profiles of Reynolds stress measured by the Gundestrup (blue) and by the U-probe (orange).**

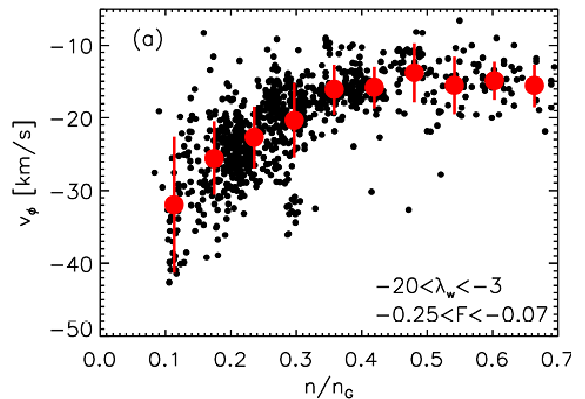


**Fig. 7: Fluctuation toroidal velocity plotted as a function of the normalized density.**

## 6. Role of coherent turbulent structures in driving transport

Understanding and controlling the mechanism driving anomalous transport is a key issue for fusion experiments. Experimental observations performed in tokamaks, stellarators, reversed field pinches and linear devices (see ref. 24 for a review) have revealed the intermittent nature common to plasma turbulence in all the different devices, and the fact that intermittency is generally associated to the presence of “blobs”, that is coherent structures, which are the result of strong nonlinearities and are generally elongated in the parallel direction.

Measurements of different electrostatic quantities, obtained with a composite insertable probe named U-probe, have been analyzed using the statistical techniques described in ref. 25, with the aim of identifying coherent structures associated to strong bursts in the fluctuation time series. Peaks on the electron pressure signal have been used as trigger. The average features of these events have then been extracted by applying the conditional average method on time window widths adequate to their time scale. The typical coherent structure detected by this method at the scale  $\tau = 3.3 \mu\text{s}$  is shown in Fig. 8. The pressure peak is accompanied by a peak of parallel vorticity  $\omega_\theta$ , so that it can be deduced that it is associated to a local velocity eddy.

The U-probe is also equipped with several magnetic probes, and this allows the unprecedented possibility of investigating the electromagnetic features of the coherent structures. Fig. 8 depicts in the last frame the parallel current density, deduced computing the parallel component of  $\nabla \times \mathbf{B}$ . A clear relation exists between the pressure structure and a peak of parallel current density. The other two components of the current density are estimated to be one order of magnitude lower, so that it can be concluded that the pressure blobs are associated to a current filament parallel to the magnetic field.

In presence of coherent structures the plasma diffusion coefficient can be separated in a part due to the plasma trapped in coherent structures  $D_p$  and another one due to the background uncorrelated turbulence [26]. The diffusivity  $D_p$  can be estimated as  $D_p \propto f_p^2 u \Delta_s$  where  $f_p$  is the packing fraction,  $u$  is the relative speed between the blobs and  $\Delta_s$  their characteristic width. This  $D_p$  definition is borrowed from the potential vortex theory [26]. The scaling of the product  $f_p^2 u \Delta_s$  with  $n/n_G$ , as measured by the GPI diagnostic, is shown in Fig. 9 for a MH plasma. In our analysis the relative speed  $u$  has been assumed to be the RMS value of the toroidal velocity  $v_\phi$  and the characteristic structure width  $\Delta_s$  has been assumed equal to the toroidal width at the higher time scale  $\tau = 10 \mu\text{s}$ , while the packing fraction has been evaluated and results about constant with  $n/n_G$ . The evaluated  $D_p$  displays a

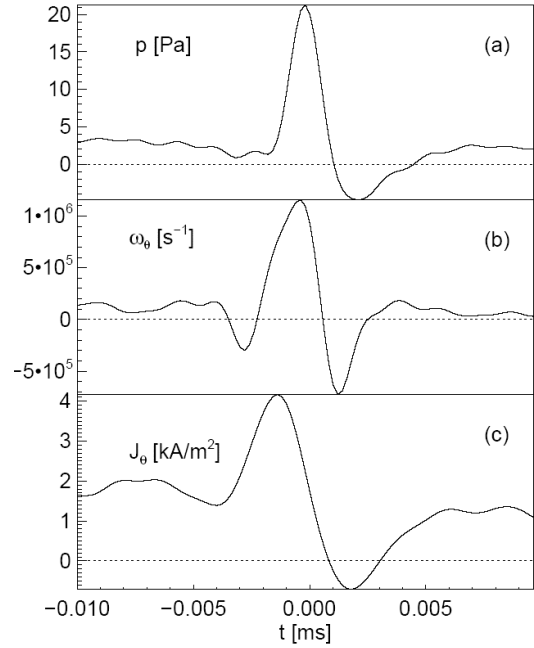


**Fig. 8: Typical coherent structure as seen on pressure, parallel vorticity and parallel current density at the scale  $\tau = 3.3 \mu\text{s}$ .**

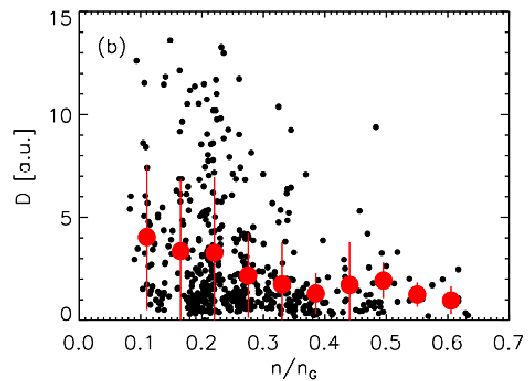


**Fig. 9: Diffusion coefficient estimated from turbulence plotted as a function of normalized density.**

decrease of about a factor 2 between discharges with low and high value of  $n/n_G$ . This result can be expounded as an increase of blob viscous damping at higher  $n/n_G$  values.

## 7. Conclusions

An overview of the most recent findings concerning the structure of the edge region and the related transport processes in RFX-mod has been presented. We have shown that the feedback system for the control of MHD modes has brought from a chaotic situation to one where conserved magnetic surfaces are present, and the  $m = 0$  islands play an important role. Typical values of the transport coefficients in low-current MH states are found to be  $D \approx 10\text{-}20 \text{ m}^2/\text{s}$  and  $\chi \approx 100\text{-}200 \text{ m}^2/\text{s}$ . The onset of QSH conditions at high current does not have a significant impact on the edge transport processes, and manifests itself mainly through an  $n = 7$  modulation of the plasma edge, which thus becomes more regular. The crucial role of microturbulence, and in particular of coherent structures and their interplay with velocity shear layers, in determining particle and momentum transport in this region has been confirmed. A new and important result is the electromagnetic nature of these structures.

This work, supported by the European Communities under the contract of Association between EURATOM/ENEA, was carried out within the framework of the European Fusion Development Agreement. The views and opinions expressed herein do not necessarily reflect those of the European Commission.

- 
- [1] FINN J. M., NEBEL R., BATHKE C., Phys. Fluids B **4** (1992) 1262.
  - [2] CAPPELLO S., PACCAGNELLA R., Phys. Fluids B **4** (1992) 611
  - [3] CAPPELLO S., ESCANDE D. F., Phys. Rev. Lett. **85** (2000) 3838.
  - [4] ESCANDE D. F., et al., Phys. Rev. Lett. **85** (2000) 1662.
  - [5] MARTIN P., et al., Nucl. Fusion **43** (2003) 1855.
  - [6] LORENZINI R., et al., Phys. Rev. Lett. **101** (2008) 025005.
  - [7] ESCANDE D. F., et al., Phys. Rev. Lett. **85** (2000) 3169.
  - [8] SONATO P., et al., Fusion Eng. Des. **66** (2003) 161.
  - [9] ZANCA P., et al., Phys. Plasmas **8** (2001) 516.
  - [10] INNOCENTE P., et al., Nucl. Fusion **47** (2007) 1092
  - [11] ZANCA P., TERRANOVA D., Plasma Phys. Control. Fusion **46** (2004) 1115.
  - [12] SPIZZO G., et al., Phys. Rev. Lett. **96** (2006) 025001.
  - [13] LORENZINI R., et al., Plasma Phys. Control. Fusion **50** (2008) 035004.
  - [14] HARVEY R. W., et al., Phys. Rev. Lett. **47** (1981) 102.
  - [15] SERIANNI G., et al., Rev. Sci. Instrum. **74** (2003) 1558.
  - [16] CARRARO L., et al., Plasma Phys Control. Fusion **40** (1998) 1021.
  - [17] MACLATCHY C. S., et al., Rev. Sci. Instrum. **63** (1992) 3923.
  - [18] JACHMICH S., et al., in Proc. 27th EPS Conference on Contr. Fusion and Plasma Phys., Budapest, 12-16 June 2000, ECA Vol. **24B** (2000) 832-835.
  - [19] ANTONI V., et al., Phys. Rev. Lett. **79** (1997) 4814.
  - [20] VIANELLO N., et al., Phys. Rev. Lett. **94**, (2005) 135001.
  - [21] AGOSTINI M., et al., Rev. Sci. Instrum. **77** (2006) 10E513.
  - [22] SCARIN P., et al., J. Nucl. Mater. **363-365** (2007) 669.
  - [23] ANTONI V., et al., J. Nucl. Mater. **313-316** (2003) 972.
  - [24] SERIANNI G., et al., Plasma Phys. Control. Fusion **49** (2007) B267.
  - [25] ANTONI V., et al., Europhys. Lett., **54** (2001) 51.
  - [26] HORTON W., ICHIKAWA Y. H., *Chaos and Structures in Nonlinear Plasmas* (World Scientific, Singapore, 1996).